

Tectonic implications of a dense continuous GPS velocity field at Yucca Mountain, Nevada

Brian Wernicke,¹ James L. Davis,² Richard A. Bennett,^{2,3} James E. Normandeau,^{2,4} Anke M. Friedrich,^{1,5} and Nathan A. Niemi¹

Received 7 October 2003; revised 3 July 2004; accepted 8 September 2004; published 15 December 2004.

[1] A dense, continuous GPS network was established in the Yucca Mountain area in 1999 to provide the most reliable measurements possible of geodetic strain patterns across the nation's only proposed permanent repository for high-level radioactive waste. The network lies astride a boundary between the geodetically stable central Great Basin and the active western Great Basin, which at the latitude of Yucca Mountain is undergoing distributed right-lateral shear at a rate of ~ 60 nstrain/yr. Monitoring from 1999 to 2003 (3.75 years) yields a velocity field characterized by nearly homogenous N20°W right-lateral shear of 20 ± 2 nstrain/yr (net velocity contrast of ~ 1.2 mm/yr across a 60 km aperture) in the vicinity of the proposed repository site. Comparison of time series of continuous results with earlier campaign surveys indicating ~ 50 nstrain/yr of west-northwest extension from 1991 to 1997 suggests that the more rapid rates were in part transient motions associated with the 1992 M_s 5.4 Little Skull Mountain earthquake. Postseismic motions do not appear to affect the 1999–2003 velocity field in either campaign or continuous data. The magnitude of the velocity contrast across the area, the overall linearity of the gradient, and the large area of undeforming crust to the east of Yucca Mountain are difficult to explain by elastic bending of the crust associated with the Death Valley fault zone, a major right-lateral strike-slip fault about 50 km west of the repository site. These observations, along with apparent local variations in the velocity gradient, suggest that significant right-lateral strain accumulation, with displacement rate in the 1 mm/yr range, may be associated with structures in the Yucca Mountain area. The absence of structures in the area with equivalent late Quaternary displacement rates underscores the problem of reconciling discrepancies between geologic and geodetic estimates of deformation rates. **INDEX TERMS:** 1208 Geodesy and Gravity: Crustal movements—*intraplate* (8110); 1243 Geodesy and Gravity: Space geodetic surveys; 8107 Tectonophysics: Continental neotectonics; 8109 Tectonophysics: Continental tectonics—*extensional* (0905); **KEYWORDS:** geodesy, tectonics, Yucca Mountain

Citation: Wernicke, B., J. L. Davis, R. A. Bennett, J. E. Normandeau, A. M. Friedrich, and N. A. Niemi (2004), Tectonic implications of a dense continuous GPS velocity field at Yucca Mountain, Nevada, *J. Geophys. Res.*, *109*, B12404, doi:10.1029/2003JB002832.

1. Introduction

[2] Yucca Mountain is one of a system of internally deformed, tilted normal fault blocks in the tectonically active Basin and Range province. At present it is the only site under evaluation by the U.S. for a permanent repository for high-level radioactive waste. Thus in addition to being

of general importance to understanding active tectonic processes, its tectonic setting is an important factor in assessing the long-term performance of both natural and engineered barriers to leakage of radioactive nuclides into the environment. Central to this assessment are the locations and rates of deformation associated with geologic features in the region such as fault zones and volcanoes. These data provide a foundation for estimating the sizes, locations and frequencies of geologic events that might be expected to occur in the region over the lifetime of the repository. These estimates may then be used to assess whether the repository will perform within regulatory standards.

[3] At a decadal or geodetic timescale, the Yucca Mountain area lies astride a boundary between right-lateral shear across the western Great Basin region and relative tectonic stasis of the central Great Basin [Bennett *et al.*, 2003] (Figure 1). The boundary between these regimes is enigmatic because it is clearly expressed in geodetic data, but

¹Division of Geological and Planetary Sciences, California Institute of Technology, Pasadena, California, USA.

²Harvard-Smithsonian Center for Astrophysics, Cambridge, Massachusetts, USA.

³Now at Department of Geosciences, University of Arizona, Tucson, Arizona, USA.

⁴Now at University Navstar Consortium, Boulder, Colorado, USA.

⁵Now at Institute for Geosciences, University of Potsdam, Potsdam, Germany.

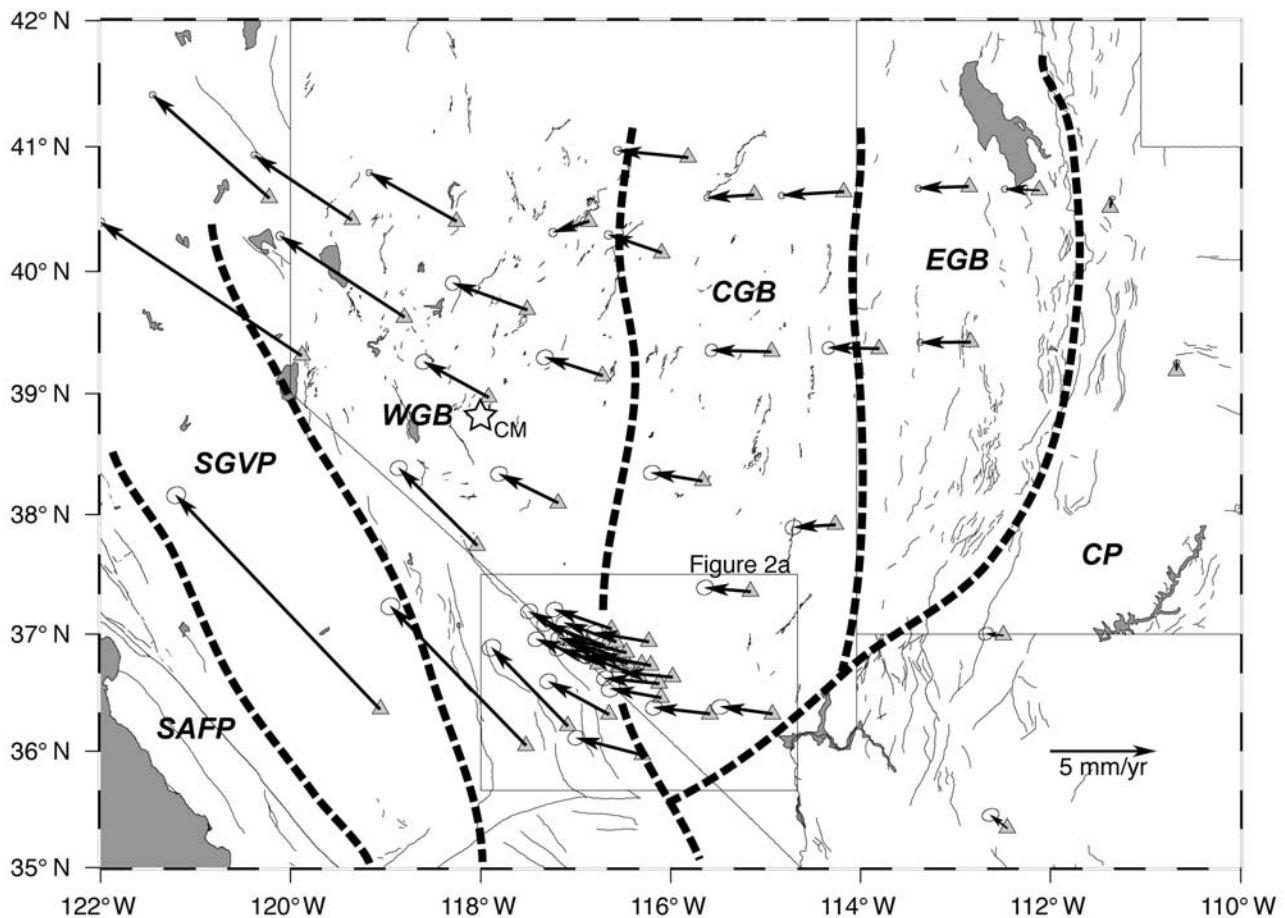


Figure 1. Map showing locations (triangles) and average horizontal velocities (arrows with 95% confidence ellipses) of continuous GPS sites of the BARGEN network. The velocities are presented in a North America-fixed reference frame [Bennett *et al.*, 2003]. Dashed lines indicate the approximate borders of the geodetic provinces from Bennett *et al.* [2003], as follows: CP, Colorado Plateau; EGB, Eastern Great Basin; CGB, Central Great Basin; WGB, Western Great Basin; SGVP, Sierra Nevada/Great Valley Province; and SAFF, San Andreas Fault Province. Star labeled CM indicates the epicenter of the 1932 Cedar Mountain earthquake. Rectangle indicates the location of the Yucca Mountain GPS network, shown in detail in Figure 2a.

does not appear to have any simple relationship to patterns of Basin and Range faulting, seismicity, or other tectonic elements. Is the boundary a relatively long-lived feature relative to earthquake recurrence intervals on Basin and Range faults (thousands to tens of thousands of years), or is it a temporary feature, such that patterns of active strain migrate across the province [Wallace, 1987]? In the latter case, geologically “instantaneous” measurements of strain accumulation and time-averaged strain release would not be well correlated. The Yucca Mountain area is well suited to examine this question, because some studies [e.g., Wernicke *et al.*, 1998] have suggested a discrepancy between relatively high levels of contemporary strain observed geodetically and relatively low strain release rates indicated from the record of late Quaternary faulting.

[4] From 1991 to 1997, seven campaign-style GPS surveys on a 35 km long, 5-site array spanning Yucca Mountain suggested west-northwest-oriented elongation of about 50 parts per billion, or 50 ± 9 nstrain/yr (nanostains per year) [Wernicke *et al.*, 1998]. The array was originally established to serve as a stable reference frame for measur-

ing deformation across rapidly moving active faults in the Death Valley region to the west. There are numerous faults with late Quaternary slip in the Yucca Mountain area, but their long-term slip rates are <0.1 mm/yr, with typical rates of order 0.01 mm/yr [e.g., Whitney and Taylor, 1996; Anderson *et al.*, 1997; Whitney and Berger, 2000; Menges and Whitney, 2002]. A nominal assumption of 10 such structures each accommodating WNW elongation of 0.01 mm/yr across the 35 km aperture of the network yields a strain rate of just 3 nstrain/yr, an order of magnitude less than the contemporary strain rate.

[5] Results from GPS surveys in 1993 and 1998 of a larger aperture (~ 50 km), 14-site network centered on Yucca Mountain indicated principal strains of 23 ± 9 nstrain/yr oriented west-northwest and -9 ± 12 nstrain/yr north-northeast averaged over the whole network, with extension reckoned positive [Savage *et al.*, 2001]. Although about a factor two lower than rates recorded by the smaller aperture, temporally denser surveys of Wernicke *et al.* [1998] over the same interval, there is substantial overlap between the two estimates at the level of 2 standard

deviations. In terms of north-northwest-oriented engineering shear strain, the reported rates for the larger network would suggest a shear strain rate of 32 ± 15 nstrain/yr. A subset of sites in the larger network that encompasses the smaller network yielded a west-northwest elongation rate of 30 ± 14 nstrain/yr [Savage *et al.*, 2001, Figure 4], which is not significantly different from the smaller array. Thus both networks indicated that significant strain was accumulating in the Yucca Mountain area, but the large uncertainties in the data left open the questions of precisely how much, and whether the strain was associated with active structures in the immediate vicinity of Yucca Mountain.

[6] Compounding the difficulty of measuring strain rates in the area, the 29 June 1992 M_s 5.4 Little Skull Mountain earthquake [Harmsen, 1994; Meremonte *et al.*, 1995; Smith *et al.*, 2001; Lohman *et al.*, 2002] occurred about 20 km east of Yucca Mountain near the beginning of the observation periods for both GPS networks, resulting in significant coseismic deformation [Savage *et al.*, 1994] and raising the possibility of significant postseismic transient strain [Wernicke *et al.*, 1998; Savage *et al.*, 1999; Savage *et al.*, 2001; Lohman *et al.*, 2002].

[7] To provide the most reliable measurements possible of active strain in the region the Yucca Mountain continuous GPS network was established in 1999. The network includes a 16-site, dense cluster focused on the Yucca Mountain area and a sparse array of some 16 sites in the surrounding region, and is a major component of the 53-site Basin and Range Geodetic Network, or BARGEN (Figure 1) [Bennett *et al.*, 1998; Wernicke *et al.*, 2000; Bennett *et al.*, 2002]. Analysis of the first three years of monitoring showed that the accuracy of the horizontal velocities from this network is among the best ever reported, with realistic uncertainties of 0.1–0.2 mm/yr [Davis *et al.*, 2003], or ± 1 –2 nstrain/yr on a 100 km baseline between two sites. Here, we use these data to determine whether the rate of deformation across Yucca Mountain is consistent with geological estimates of strain rate, and to address the question of whether significant strain is associated with structures in the Yucca Mountain area, once the effects of right-lateral shear on the Death Valley fault zone ~ 50 km to its west (Figure 2) are accounted for.

2. Regional Tectonic Setting

[8] Geodetic solutions for the entire BARGEN network show increasing west velocities (with respect to a nominal North American reference frame) across the eastern part of the Great Basin in Utah, relatively constant velocities across the central Great Basin, and increasing

northwest velocities across the western Great Basin in western Nevada and eastern California (Figure 1). As mentioned above, the Yucca Mountain area lies along a north-trending boundary between two provinces identified on the basis of these geodetic patterns (Figure 1). To the east of Yucca Mountain, occupying most of Nevada east of longitude 116.5°W , lies the central Great Basin geodetic province, wherein the average velocity of all sites is 2.8 mm/yr and there are no significant systematic variations in velocity (Figure 1). To the west of the boundary lies the western Great Basin geodetic province, wherein velocities systematically increase from east to west, giving an overall north-northwest right-lateral shear relative to the central Great Basin province. The total right shear across this province, or the motion between the Sierra-Great Valley and central Great Basin provinces, is 9.3 mm/yr [Bennett *et al.*, 2003]. Because of the high density of continuous sites deployed across the boundary, the Yucca Mountain cluster provides an especially rich opportunity to understand the details of the transition between two major geodetic provinces, and address the question of how the boundary is expressed, if at all, by late Quaternary structures in the area.

[9] Geologically, the Yucca Mountain area is located within the Walker Lane belt [e.g., Stewart, 1988], a portion of the southwestern Great Basin defined on the basis of complex patterns of basins and ranges that contrast with the more orderly pattern elsewhere. The Yucca Mountain area lies just east of the Eastern California shear zone, a region defined on the basis of late Cenozoic right-lateral faulting [Dokka and Travis, 1990]. The boundaries of these tectonic elements, as defined, are not necessarily coincident with boundaries between regions defined on the basis of geodetic patterns [Bennett *et al.*, 2003, Figures 1, 10], which raises the general question of how long-lived the geodetically defined boundaries are.

[10] At the latitude of Yucca Mountain, shear within the western Great Basin geodetic province is dominated by three north- to northwest-striking strike-slip fault zones (Figure 2a). From west to east these include the Owens Valley, Panamint Valley, and Death Valley fault zones [e.g., Dokka and Travis, 1990; Dixon *et al.*, 1995; Hearn and Humphreys, 1998; McClusky *et al.*, 2001]. Early campaign GPS surveys demonstrated that the total right-lateral displacement rate across this zone is of order 10 mm/yr, with a gradient in velocity of ~ 60 nstrain/yr across the traces of the three faults [e.g., Bennett *et al.*, 1997; Dixon *et al.*, 2000; Gan *et al.*, 2000; Miller *et al.*, 2001; McClusky *et al.*, 2001]. Geologically determined rates of late Quaternary right-lateral slip on each of these faults typically range from ~ 2 to 5 mm/yr, although the upper bounds of some estimates are greater [e.g., Dixon *et al.*, 1995; Reheis and

Figure 2. (a) Shaded relief map showing the horizontal velocity field for the Yucca Mountain GPS network. Sites are located at the base of the velocity arrows, shown with 95% confidence ellipses. Quaternary faults are shown with thin lines. Principal right-lateral strike-slip faults are labeled as follows: OVFZ, Owens Valley fault zone; HMFZ, Hunter Mountain fault zone; PVFZ, Panamint Valley fault zone; DVFZ, Death Valley fault zone; PSFZ, Pahrump-Stateline fault zone. (b) Inset showing details of the horizontal velocity field for the Yucca Mountain cluster. Locations of sites MILE and WAHO are indicated by white triangles. Star indicates the epicenter of the 29 June 1992 M_s 5.4 Little Skull Mountain earthquake. Dashed lines in Figures 2a and 2b indicate the location of the model Death Valley fault discussed in text.

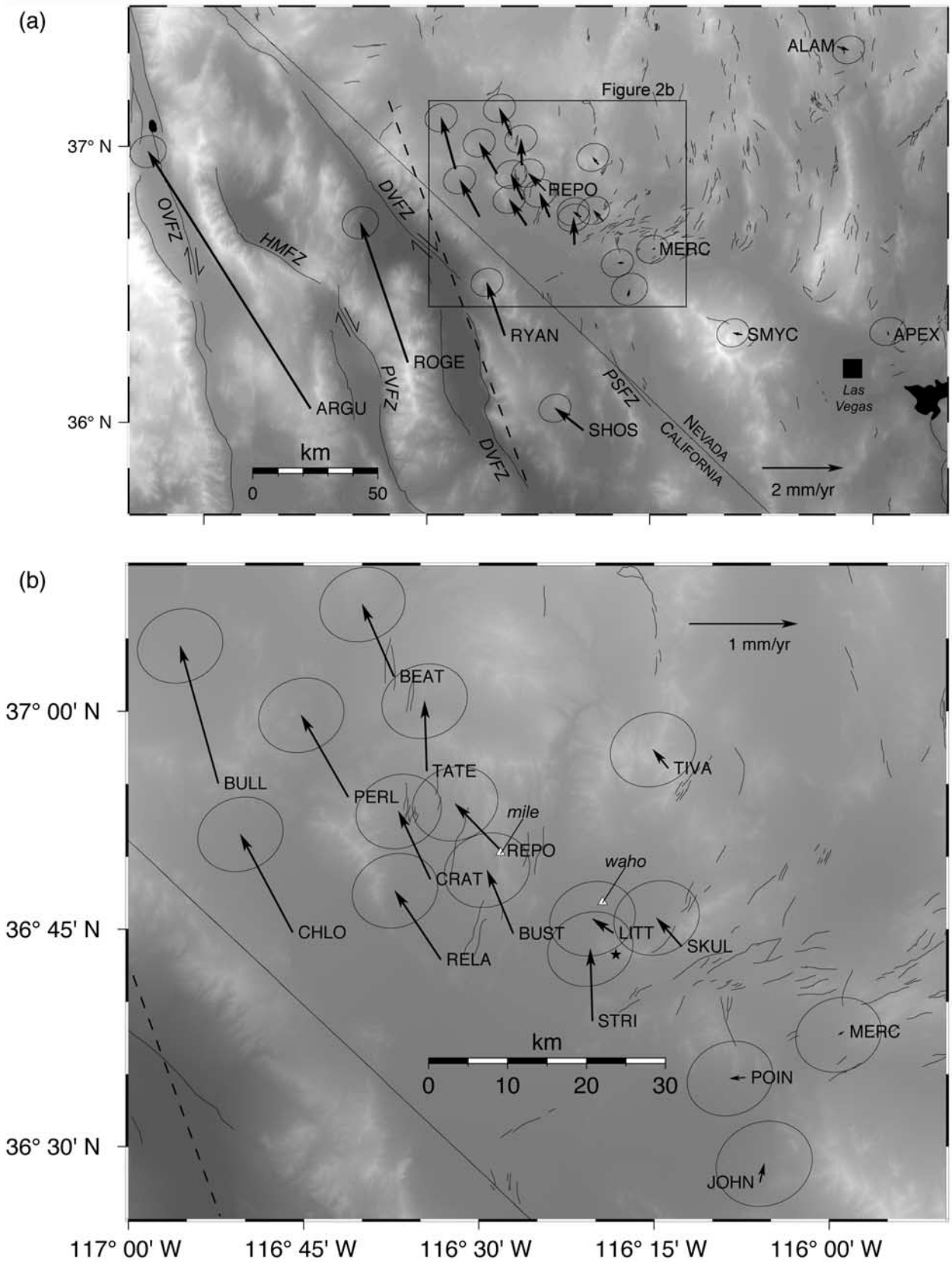


Figure 2

Dixon, 1996; Reheis and Sawyer, 1997; Klinger and Piety, 2000; Lee *et al.*, 2001].

3. Geodetic Data

[11] The geodetic velocities of our continuous sites (Figure 2) were determined using daily position estimates from mid-1999 through early 2003, or about 3.75 years, here updated from earlier solutions [Bennett *et al.*, 2003; Davis *et al.*, 2003]. All BARGEN sites consist of choke ring antennae mounted on Wyatt design braced monuments anchored in bedrock from a depth of 5 to 10 m to minimize local site motion [Langbein *et al.*, 1995; Bock *et al.*, 1997; Wernicke *et al.*, 2000]. GPS phase data were collected every 30 s on Trimble 4000 series receivers and 24 hr data sets were remotely downloaded daily.

[12] Geodetic solutions for position and velocity were generated using the GAMIT/GLOBK software, following methods previously detailed by Bennett *et al.* [2002]. We incorporated into our solution data products from other continuous GPS networks, including the International GPS Service (IGS) and Bay Area Regional Deformation (BARD) networks, obtained from the Scripps Orbit and Permanent Array Center (SOPAC). Our model for site velocities accounts for time series offsets near the beginning of monitoring at the epochs of equipment changes (primarily the addition of radomes to the antennae in August 1999) and coseismic effects of the 16 October 1999 M_w 7.1 Hector Mine earthquake \sim 200 km to the south of the cluster [e.g., Simons *et al.*, 2002]. Postseismic effects of this event have not been taken into account in the solution, but the event was sufficiently distant as to affect strain rate estimates across the network at <1 nstrain/yr (T. Herring, oral communication, 2004). Error ellipses in Figures 1 and 2 are 95% confidence limits based on formal standard deviations scaled (by a factor of 2) to yield a reduced χ^2 of unity for the simple two-region constant strain rate model used by Davis *et al.* [2003] and discussed further below.

[13] The transition between geodetic stability in the central Great Basin province and right-lateral shear in the western Great Basin province is defined by viewing the velocity field in a reference frame that minimizes the motions of the four easternmost sites in the area ALAM, APEX, SMYC and MERC (Figure 2a). Within the cluster, from east to west, sites POIN and JOHN are relatively stationary in this frame, and sites SKUL, TIVA and LITT have northward velocities of a few tenths of a millimeter per year, and thus appear to define the eastern margin of resolvable right-lateral shear. The remaining 10 sites to the west within the cluster have significant north-northwest velocities, increasing to 1.3 mm/yr for the westernmost site, BULL.

[14] The increase is apparent in the filtered [e.g., Wdowinski *et al.*, 1997] north components of representative time series for three of the sites in the cluster, site MERC on the east side of the shear zone, site REPO, which lies within the gradient (and directly on top of the proposed waste repository), and site BULL to the west (Figures 2 and 3). The resulting root-mean-square (rms) scatter in both east and north daily position estimates ranges from 0.6 to 0.9 mm. The north components of these time series progressively increase by a total of 1.2 mm/yr between sites MERC and BULL.

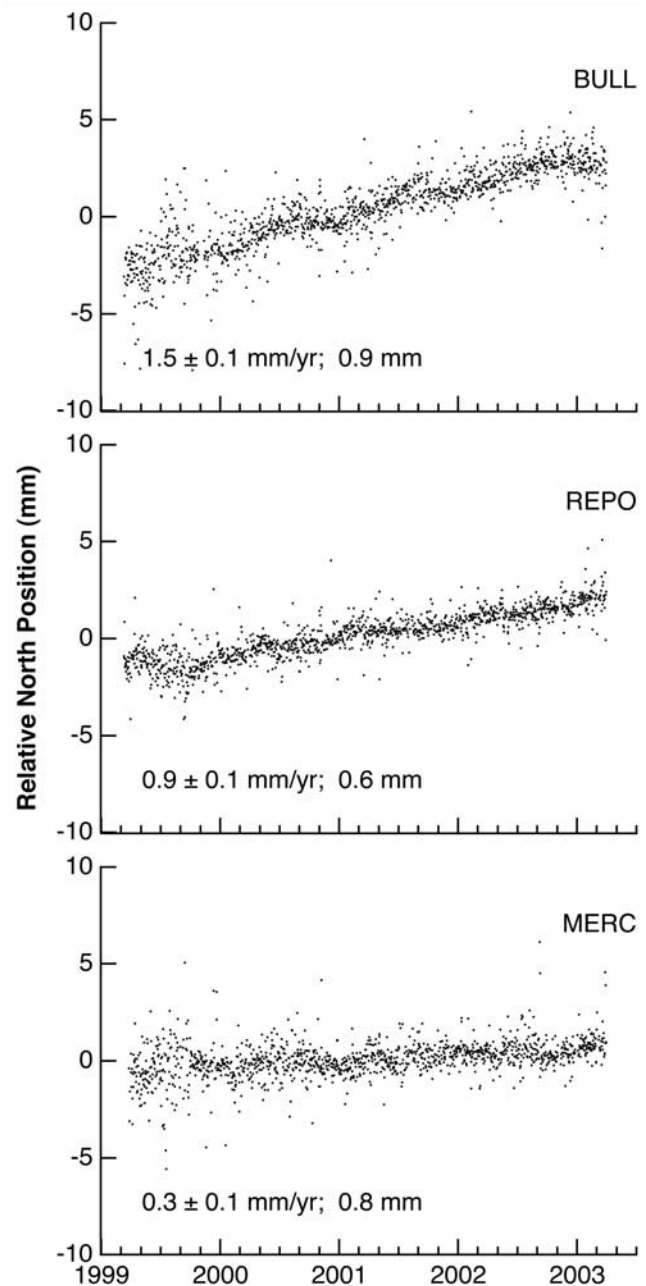


Figure 3. Filtered [e.g., Wdowinski *et al.*, 1997] time series for the north components of position for three sites in the Yucca Mountain cluster, illustrating increasing northward velocity with westward position. Values shown are relative to respective nominal average values in a North America-fixed reference frame. For clarity, the error bars are not shown but are generally \sim 2 mm. The best fit slopes and (formal) uncertainties and the weighed root-mean-square residual are shown. The rates obtained from the slope to the time series differ slightly from the vector velocity values shown in Figures 1 and 2. The vector velocities are calculated using a Kalman filter [Herring *et al.*, 1990] that rigorously accounts for statistical correlations. The calculation of the time series slopes neglects the correlations among the site position estimates for different sites and epochs, because using them in the analysis is computationally impractical.

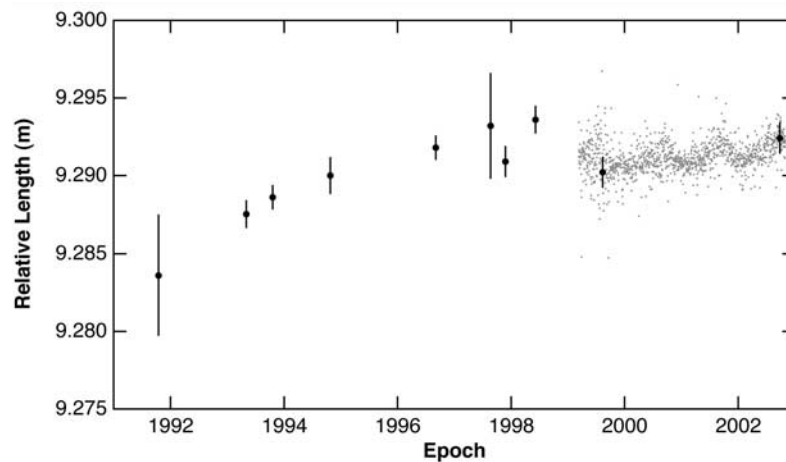


Figure 4. Time series of MILE-WAHO line length estimates (filled circles with 1σ error bars) relative to the value 14,440 m. REPO-LITT line length estimates (gray dots) are shown after adjustment for the offset from the MILE-WAHO length using the last two MILE-WAHO observations, obtained during the period of continuous GPS surveys. The small (~ 0.4 mm) seasonal signature in the REPO-LITT baseline evolution appears to be associated with a like-amplitude variation of the LITT east component.

[15] In addition to our continuous GPS measurements, two 24-hour surveys of two standard geodetic markers, sites MILE and WAHO (see locations on Figure 2b) were conducted in 1999 and 2002, for comparison with the 1991 to 1997 measurements [Wernicke *et al.*, 1998] discussed above, which included both of these sites. Because the cluster was operating during the 1999 and 2002 surveys, we can estimate the position of sites WAHO and MILE within the continuous network, and compare the history of line length changes with two nearby continuous sites, including site REPO, which is only a few hundred meters from site MILE, and site LITT, which is about 4 km south of site WAHO (Figure 2b).

[16] Both the repeated campaign measurements of the WAHO-MILE baseline from 1997 to 2002 and the continuous measurements from 1998 to 2002 indicate a lower rate of line lengthening than the campaign measurements from 1991 to 1997 (Figure 4). Lohman *et al.* [2002] used a joint inversion analysis of seismic waveform data and InSAR data to estimate the source parameters and coseismic surface displacement field for the 1992 Little Skull Mountain earthquake, which indicates coseismic lengthening of the WAHO-MILE baseline by 5 ± 1 mm, consistent with the value of 3 ± 3 mm determined directly from the campaign GPS data [Wernicke *et al.*, 1998]. Adjusting the preseismic, 1991 survey by 5 mm, we find that the average strain rate based on line length change from 1991 through 1997 was 0.8 ± 0.2 mm/yr (59 ± 14 nstrain/yr), consistent with the results based on the two USGS campaigns in 1993 and 1998 of the same monuments, plus several others nearby, which as mentioned above yielded an average local strain rate across Yucca Mountain of 30 ± 14 nstrain/yr [Savage *et al.*, 2001]. If we consider only the five surveys spanning 1997 through 2002, the rate is significantly lower, at 0.0 ± 0.3 mm/yr, in agreement with the REPO-LITT rate of 0.3 ± 0.1 mm/yr (Figure 4). The anomalous rates from the 1991 to 1997 surveys therefore appear to define a 6 year interval of transient accelerated strain, possibly associated with fault

afterslip or viscoelastic relaxation following the 1992 Little Skull Mountain earthquake, or some other transient process.

[17] Outside the cluster, sites to the south and west, including SHOS, RYAN, ROGE and ARGU, continue the pattern of increasing north-northwest velocity, consistent with previously published results based on campaign data [Bennett *et al.*, 1997; Dixon *et al.*, 2000; Gan *et al.*, 2000; Miller *et al.*, 2001]. Within the deforming part of the cluster (all sites of Figure 2b except POIN, MERC, and JOHN), the observed velocity gradient components are $\pm \partial v_e / \partial x_e = 5 \pm 2$ nstrain/yr, $\partial v_e / \partial x_n = 2 \pm 3$ nstrain/yr, $\partial v_n / \partial x_e = -16 \pm 2$ nstrain/yr, and $\partial v_n / \partial x_n = -4 \pm 3$ nstrain/yr, where subscripts e and n refer to east and north, respectively. The resulting principal strain rates are of equal magnitude (within their uncertainties) and opposite sign, consistent with horizontal simple shear. The axis of maximum principal strain within the cluster is $N62^\circ \pm 6^\circ W$, with right-lateral shear directed along $N17^\circ \pm 6^\circ W$ (scaled standard deviations), in good agreement with the overall orientation of strike-slip faults within the western Great Basin geodetic province. The overall direction of shear is therefore perhaps best represented by the motion of site ROGE, which is moving $19^\circ \pm 7^\circ$ west of north, parallel to the direction of RYAN and the average direction of sites in the western part of the cluster (Figure 2a). The direction of motion of ARGU is slightly more west of north at $N32^\circ \pm 4^\circ W$ perhaps reflecting a component of transtension across the Panamint Valley/Hunter Mountain fault zone.

4. Discussion

4.1. Strain Pattern

[18] The Death Valley fault zone is the most conspicuous active geologic structure that would contribute to the strain pattern across Yucca Mountain. A key concern in assessing the geophysical significance of this data is whether the velocity field is entirely the result of intermediate- to far-field elastic bending of the crust adjacent to the Death Valley fault zone and faults farther west, or whether it

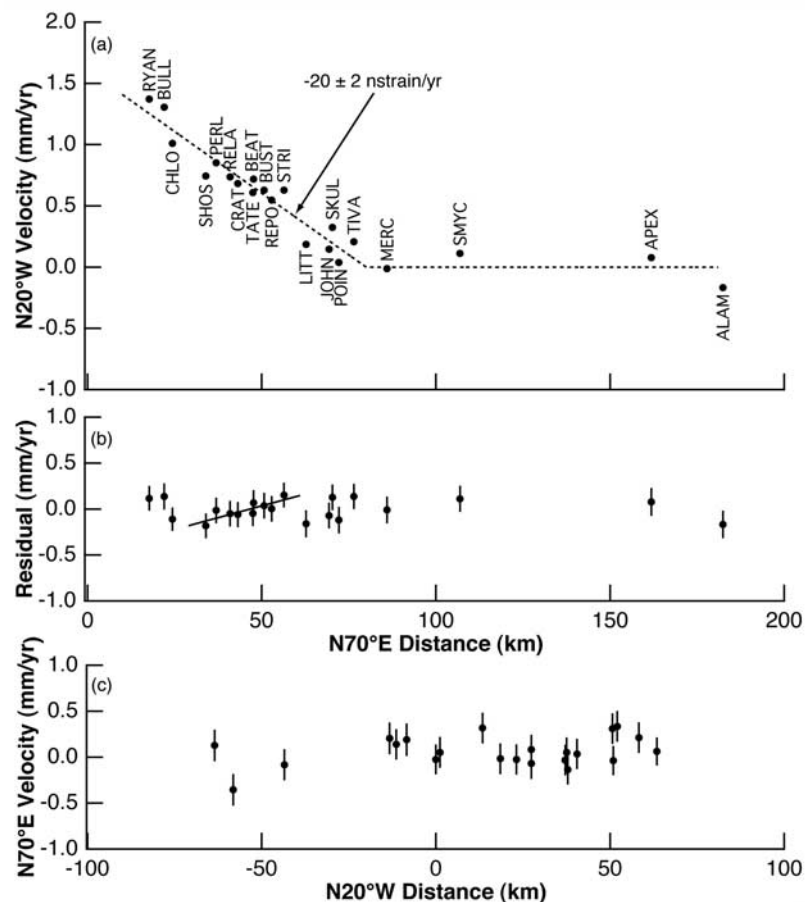


Figure 5. (a) Site velocities projected onto the N20°W direction, plotted as a function of distance along the N70°E direction. Error bars have been omitted for clarity. The dashed line is the best fit model composed of a constant strain rate for negative distance values and zero strain rate for positive distance values. The $x = 0$ coordinate represents the estimated location of the transition from shearing to nonshearing deformation. (b) Post-fit residual velocities. Note the difference in vertical scale. Line shows linear regression of velocities of sites between SHOS and STRI, as discussed in text. See Figure 5a for site name. (c) Site velocities projected onto the N70°E direction, plotted as a function of distance along the N20°W direction. Error bars (Figures 5b and 5c) are 2σ (see text).

reflects near-field strain accumulation on active structures within the Yucca Mountain area. Therefore, following the approach of *Savage et al.* [1999] we use these data to test whether simple models of elastic bending reasonably explain the velocity profile across Yucca Mountain, or alternatively whether a significant amount of the strain is related to other processes, such as viscoelastic effects from earthquakes or additional, albeit less obvious structures within the Yucca Mountain area itself. In the analysis below, we adopt N20°W for the direction of shear relative to the central Great Basin geodetic province and use variations of N20°W components of velocity in the direction N70°E to estimate horizontal gradients in shear strain in the region.

[19] To first order, across Yucca Mountain the gradient in N20°W velocity is relatively constant (Figure 5a). The east margin of the gradient appears to lie within the group of sites MERC, JOHN and POIN. Because SKUL and TIVA have marginally significant velocity and are the same distance measured N70°E from the Death Valley fault zone as POIN and JOHN, the east-northeast limit of measurable

shear lies somewhere within this group of sites, or about 65 to 75 km east-northeast of the Death Valley fault zone near the eastern margin of the cluster (Figure 2a).

[20] Across the cluster, over a distance of 50 to 60 kilometers, the velocity increases by about 1.2 mm/yr. Linear regression of N20°W components of all sites within the deforming region of the cluster (taking it to exclude site MERC but include sites TIVA, POIN, and JOHN) yields a right-lateral shear strain rate of 20 ± 2 nstrain/yr (Figure 5a). The residual components of velocity for both north-north-west homogeneous shear and for motions normal to the shear zone exhibit scatter in velocity of 0.14 mm/yr RMS (Figure 5b), in agreement with the value from *Davis et al.* [2003] from a shorter data set, but a factor of two greater than expected for this data set. This result may indicate a systematic error of ~ 0.1 mm/yr associated either with the position estimates or, more likely (given the *Davis et al.* [2003] results) with the simple model of linear strain rate variation. Viewed in a larger context, the strain gradient across Yucca Mountain is smaller than that immediately to

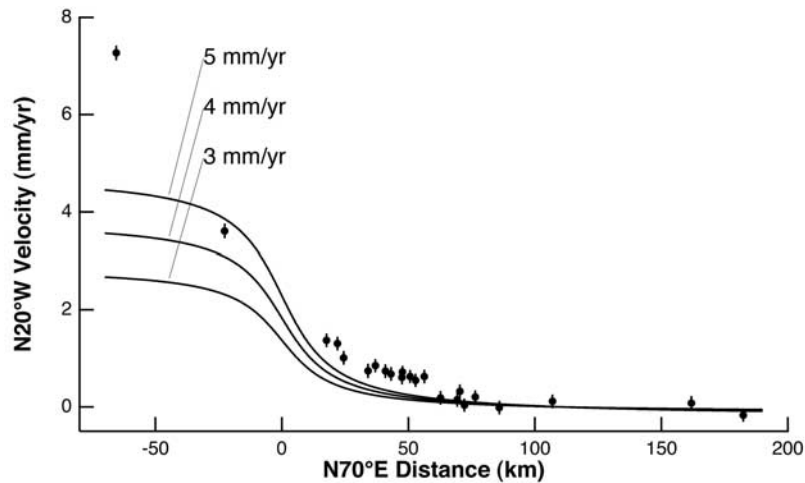


Figure 6. Observed velocities from Figure 5a, with scale expanded to include sites ROGE and ARGU. See Figure 5a for site names. The solid lines indicate the modeled fault-parallel velocity for the adopted position (Figure 2) and parameters assumed for the Death Valley fault discussed in the text, with three different slip rate values indicated. In the coordinate system of Figure 6 the fault is located at $x = 0$ km. The model velocities have been adjusted with an additive offset to yield an average velocity of zero between sites MERC and ALAM (inclusive) to match the GPS velocity reference frame.

the west, as shown by a plot scaled to include sites ROGE and ARGU (Figure 6).

[21] Although the scatter about a linear regression within the gradient is small, there is some indication that it is at least locally systematic. In particular, the residual N20°W velocities for the group of sites between SHOS and STRI appear to increase progressively eastward (Figures 5a and 5b). On the plot of N20°W velocity (Figure 5a) this appears as a gradient that is approximately half that of the linear model for these sites (linear regression yields 10 ± 3 nstrain/yr for these sites), with velocity dropping off relatively abruptly to the east. A lower velocity gradient for these sites implies an eastward increase in the velocity gradient in the vicinity of sites STRI and LITT. Indeed, in map view (Figure 2b), a locally steep velocity gradient is apparent in this area, with relatively low velocities east of and including site LITT, and relatively high velocities west of and including site STRI.

4.2. Dislocation Models of the Death Valley Fault Zone

[22] Are simple strain accumulation models involving only the Death Valley fault zone consistent with the data? For the purpose of this discussion, we will model the Death Valley fault as a locked fault above an infinitely long buried strike-slip dislocation. To maximize the influence of the model on the Yucca Mountain area, we choose a locking depth of 15 km, based on the maximum hypocentral depths determined for some 6000 earthquakes in the southern Great Basin region from 1978 to 1992 [von Seggern and Brune, 2000]. We adopt a strike for the Death Valley fault zone of N20°W, and a position where its trace comes closest to the cluster in an east-northeast direction, where it bends from a north-south to a northeast orientation 55 km west-southwest of site STRI (Figure 2b). In this position, the surface trace of the fault is mostly at a greater distance from the cluster than the model dislocation. Other parameters follow those used by Savage *et al.* [1994, 1999].

[23] In Figure 6, we show models for slip rates of 3, 4 and 5 mm/yr as representative of the range of probable late Quaternary slip rates on the Death Valley fault zone based on previous geologic and geodetic analyses [Dixon *et al.*, 1995, 2000; Reheis and Dixon, 1996; Reheis and Sawyer, 1997; Bennett *et al.*, 1997; Hearn and Humphreys, 1998; Klinger and Piety, 2000; Miller *et al.*, 2001]. None of these models fit the data, with all 12 sites in the cluster west-southwest of LITT lying well above the curve for a 5 mm/yr slip rate. Even the 5 mm/yr curve explains only $\sim 50\%$ of the velocity for sites in the middle of the cluster, such as sites CRAT and BEAT, relative to far field sites to the east.

[24] Adjusting the locking depth upward, the position of the fault farther to the west, or adopting a lower slip rate than 5 mm/yr, all of which we regard as likely, increases the mismatch between model and data. For example, moving the model fault 10 km west-southwest (where it best averages the position of the fault trace), decreasing the locking depth to 12 km (the depth limit of 95% of all earthquakes in the region) and assuming a rate of 3.5 mm/yr (following Reheis and Dixon [1996, Figure 4]), the contribution of the model Death Valley fault zone to the velocity of sites CRAT and BEAT is only $\sim 10\%$.

[25] Model slip rates in excess of 5 mm/yr result in a significant overestimate of the observed velocity of site ROGE. In addition, because site ROGE lies immediately east of the Panamint Valley/Hunter Mountain fault zone (Figure 2a) with a Holocene slip rate of 2.4 ± 0.8 mm/yr [Zhang *et al.*, 1990], a significant fraction of its velocity is likely associated with that fault zone [Dixon *et al.*, 1995]. Therefore a slip rate for the Death Valley fault zone of 5 mm/yr is an upper limit if these models are applicable.

[26] Perhaps the greatest difference between these models and the data within the cluster—which the accuracy of dense, continuous data is well suited to address—is the fact that elastic bending models predict relatively high, negative

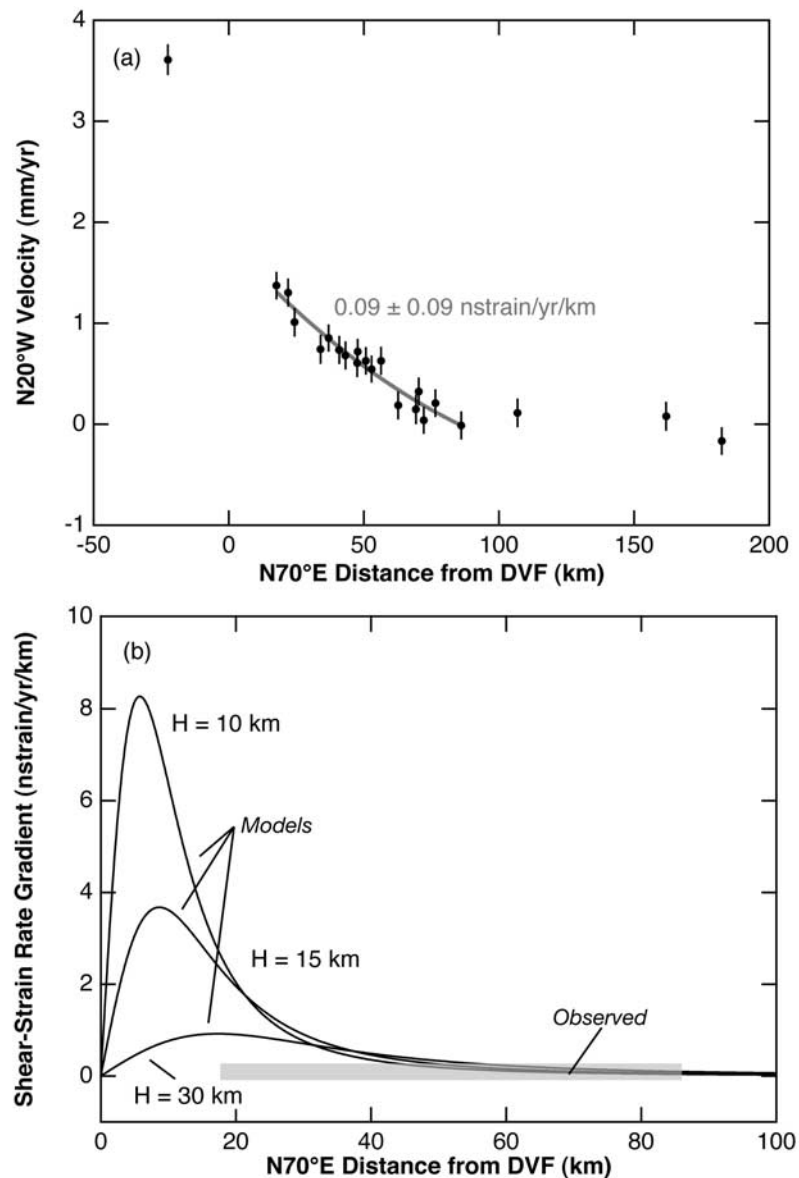


Figure 7. (a) N20°W velocities for all sites except ARGU. Model Death Valley fault (Figure 2) has the horizontal coordinate value $x = 0$. The gray line is the best fit second-order polynomial. The value of the coefficient of the quadratic term, which represents the shear strain rate gradient, is also shown in gray. (b) Predicted shear strain rate gradient for three models for the Death Valley fault having different locked-zone depths H . Note the change in both horizontal and vertical scales from Figure 7a. The value for the observed (constant) shear strain rate gradient is shown as a gray line of width 1σ .

strain rate gradients (i.e., systematic decrease in strain rate, or systematic curvature of the velocity field) in the intermediate (5–30 km) to far (>30 km) field from the fault, whereas the observed gradient across the cluster is constant. A fit of the data within the cluster to a second-degree polynomial yields a negligible overall curvature of 0.09 ± 0.09 nstrain/yr/km (Figure 7a), whereas the values predicted by these models are 1 to 2 orders of magnitude higher, depending on position within the cluster (Figure 7b). Perhaps the somewhat lower gradient within the cluster is a reflection of these models, but if so it implies an increase in strain rate to the east, as mentioned above. Hence we conclude that simple models of elastic bending of the crust

adjacent to the Death Valley fault zone are not sufficient to explain the overall strain pattern within the cluster.

4.3. Alternative Models

[27] Perhaps the simplest alternatives to a single fault 50 km to the west are (1) transient deformation due to nearby earthquakes or (2) a two-fault dislocation model, with a second fault closer to Yucca Mountain.

[28] The two most significant earthquakes in regard to postseismic relaxation in the Yucca Mountain area are the 1992 Little Skull Mountain event and the 1872 $M \sim 7.6$ Owens Valley event [Beanland and Clark, 1994]. The network covers a relatively large aperture relative to the Little

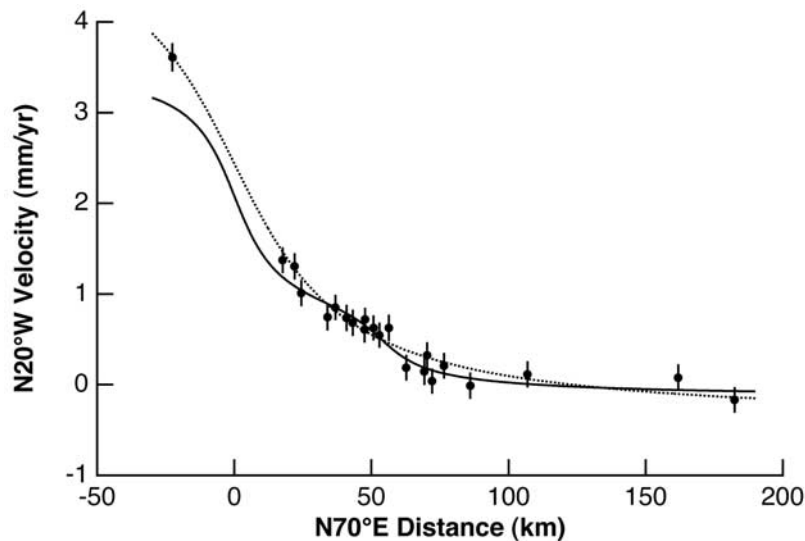


Figure 8. N20°W velocities and the two-fault model described in the text (solid curve). The coordinate system is the same as that of Figures 7 and 8. The second fault is located at $x = +54$ km. The model velocity curve has been adjusted into the GPS reference frame as described in the caption for Figure 6. Dotted curve shows single fault at $x = 0$ with 30 km locking depth and slip rate of 5.75 mm/yr.

Skull Mountain earthquake, which was only M_s 5.4. Its focal mechanism was normal to left oblique normal [e.g., *Lohman et al.*, 2002]. Notwithstanding the postseismic signal near the center of the cluster, the event would be unlikely to impose significant right-lateral transient strain across the cluster. With a rupture dimension of only ~ 5 km [*Lohman et al.*, 2002], it would be unlikely to have a significant effect over the entire cluster, which has a width of about 10 rupture dimensions (Figure 2). As for the 1872 event, *Dixon et al.* [2000, 2003] argued that the discrepancy between geodetic and geologic velocities in the Owens Valley (geodetic velocities being higher) results from transient accelerated displacements of several mm/yr in the epicentral region, nearly 130 years after the event. However, the Yucca Mountain GPS cluster is 100 to 150 km (~ 10 rupture dimensions) from the Owens Valley rupture (Figure 2a), and as such the postseismic effect would be either left-lateral or negligible at the position of the cluster [e.g., *Savage*, 2000, Figure 3a; *Dixon et al.*, 2003]. Therefore the 1872 event is unlikely to be a source of enhanced right-lateral shear across the cluster. We therefore conclude that accelerated transient deformation due to postseismic viscoelastic relaxation is an unlikely explanation for the velocity gradient across the cluster.

[29] As mentioned above, there is ample evidence of late Quaternary faulting within the area of the cluster, but individual faults have slip rates of much less than 0.1 mm/yr. Southeast of the cluster, some 60 km east of the southern part of the Death Valley fault zone, there is a relatively continuous northwest striking Quaternary structure known as the Pahrump-Stateline fault zone (Figure 2a) [*Stewart*, 1988; *Schweickert and Lahren*, 1997]. The fault zone is traceable to a point about 40 km south of site MERC. North of this point, there are a number of Quaternary faults of diverse orientation, but there is no throughgoing, northwest striking fault offsetting surficial deposits. *Schweickert and Lahren* [1997] proposed, on the basis of subsurface data, gravity anomalies, spring alignments and other criteria that the fault

continues northward in the subsurface toward the Yucca Mountain area as the “Amargosa Desert fault system,” where it is expressed at the surface by diffuse faulting and block rotation. This model may be in accord with the observation that no individual structure in the Yucca Mountain area has an appreciable slip rate, as discussed further below.

[30] To account for the relatively high strain rates at Yucca Mountain using simple dislocations, models with more than a single dislocation are required. As just one example, we are able to provide an excellent fit to the velocity data with two buried dislocations with locking depths at 12 km, one representing the Death Valley fault zone with a slip rate of 2.8 mm/yr [e.g., *McClusky et al.*, 2001], and another representing the Stateline-Pahrump and proposed Amargosa Desert fault system (assumed strike N20°W) with a slip rate of 0.9 mm/yr, centered in the Fortymile Wash area between sites LITT and STRI (Figure 8). This is just one of many such models using two or more buried dislocations that could provide a reasonable fit to the velocity data. However, this particular model does account for the apparent local variations in strain rate in the vicinity of sites LITT and STRI discussed earlier.

[31] Models consisting of a wide zone of homogeneous simple shear in the upper mantle [e.g., *Bourne et al.*, 1998] could also explain the observed deformation. These models assume that strain accumulation at the surface is a direct measure of permanent strain at depth, and therefore predict that geologic estimates sum directly to yield geodetic estimates.

[32] More sophisticated, two- and three-dimensional models that incorporate complexities in fault geometry, long-term seismic cycle effects and variations in rheologic parameters [e.g., *Hager et al.*, 1999; *Helland and Hager*, 2003] are also possible. For example, a two-dimensional viscoelastic coupling model extended to account for long-term seismic cycle effects on the Owens Valley, Panamint Valley/Hunter Mountain and Death Valley faults predicts a relatively gradual

variation in velocity across the cluster of about 1.5 mm/yr [Dixon *et al.*, 2003, Figure 2]. This model predicts that the Death Valley fault is late in its seismic cycle, yielding a much broader distribution of strain than is predicted by simple dislocation models, akin to the effect of a very deep locking depth. Although this particular model is successful at explaining the relatively high gradient within the western part of the cluster, about half of the velocity variation in the model (~ 0.8 mm/yr) occurs east-northeast of site LITT, which is at least a factor of 3 greater than the observed variation (Figure 2b). However, models of this general type may explain the data. For example, a simple dislocation model for the Death Valley fault with a locking depth of 30 km and slip rate of 5.75 mm/yr provides a reasonable fit to the data (Figure 8).

[33] Discriminating among models such as these will require a rigorous paleoseismic investigation of the Pahrump-Stateline and Death Valley fault zones to determine the modern context of the Yucca Mountain area within the seismic cycles of these faults, and whether their slip rates sum to match geodetic rates. Modeling efforts would also benefit from denser geodetic coverage across both fault zones.

4.4. Migratory Strain Accumulation Versus Distributed Inelastic Yielding

[34] The possibility of active structures east of the Death Valley fault zone with contemporary displacement rates in the 1 mm/yr range, versus the lack of evidence for geologic structures that could sustain such rates raises the possibility that strain accumulation and release in the Basin and Range periodically migrates from region to region [Wallace, 1987]. In general, the low geologic deformation rates of active structures in the Yucca Mountain area are similar to those observed throughout large areas of the eastern, central and western Great Basin geodetic provinces. Syntheses of paleoseismic data indicate that late Quaternary displacement rates on the largest Basin and Range faults, located well outside the Yucca Mountain area, are typically 0.1 to 0.3 mm/yr [e.g., Niemi *et al.*, 2004; Friedrich *et al.*, 2003]. The apparent mismatch between geodetic and geologic rates may suggest that the Yucca Mountain area is experiencing a transient period of strain accumulation greater than its average strain release rate, with such transients periodically "visiting" the region and activating its structures [Wernicke *et al.*, 1998]. If the ~ 1 mm/yr rate is not transient on geologic timescales, then only a small fraction of strain release in the area is being accommodated on discrete structures whose displacement rates are observable through examination of surficial deposits. If so, then a large proportion of strain release occurs by diffuse inelastic yielding, and is therefore very difficult to measure using geological methods.

[35] Again, these hypotheses may be evaluated by determining the late Quaternary displacement rate across the Stateline-Pahrump fault zone, where deformation east of the Death Valley fault zone appears to be most discrete. A geologic offset rate of 0.1 mm/yr on this structure would favor the transient strain accumulation hypothesis, while a 1 mm/yr rate would favor absorption of strain to the north in the Yucca Mountain area on structures too diffuse to clearly record it. Either hypothesis predicts more strain release over the next 10,000 to 100,000 years than would be predicted by examination of the geologic history alone [Wernicke *et al.*, 1998].

[36] If ~ 1 mm/yr of strain is accumulating in the area, how is it likely to be released? For comparison purposes, a discrete strike-slip fault straining at 20 nstrain/yr across the 60 km aperture of the GPS cluster would accumulate a total right-lateral displacement of 120 m in the next 100,000 years, which would require about 40 large ($M \sim 6.5$ to 7.5) earthquakes to release. Because no such structure exists in the Yucca Mountain area, surface strain release for each event would presumably be expressed as slip on an array of smaller ruptures.

[37] As previously recognized [Bell *et al.*, 1999, and references therein] the closest analogy to the type of event that could accommodate significant strain accumulation in the Yucca Mountain area is the 1932 M_s 7.2 Cedar Mountain earthquake. The Cedar Mountain area is about 200 km north-northwest of Yucca Mountain (Figure 1). It is in an analogous position along the northeast margin of the Walker Lane belt, within a portion of the western Great Basin geodetic province with regional strain accumulation estimated at 25 ± 5 nstrain/yr [Bennett *et al.*, 2003], and local engineering shear strain rate estimated at 58 ± 12 nstrain/yr [Savage *et al.*, 1995]. The Cedar Mountain earthquake was a right-lateral strike-slip event, expressed as a wide, complex, semicontinuous pattern of distributed strike-slip and normal-slip surface ruptures cutting across a complex topographic pattern for a distance of about 75 km. Paleoseismic investigations suggest an average recurrence rate of similar events every 3,600 years [Bell *et al.*, 1999]. Bell *et al.* [1999, p. 791] concluded that

In contrast to most other historical events in the Basin and Range province, the 1932 event did not occur along a major range-bounding fault, and no single, throughgoing basement structure can account for the observed rupture pattern. The 1932 faulting supports the concept that major earthquakes in the Basin and Range province can exhibit complicated distributive rupture patterns and that slip rate may not be a reliable criterion for modeling seismic hazard.

Given the complicated pattern of low slip rate faults in the Yucca Mountain area, our results suggest earthquake scenarios along the lines of the Cedar Mountain event should be given significant weight in modeling seismic hazard in the Yucca Mountain area. Such an event would be expected every few thousand years, so long as the contemporary pattern of strain accumulation continues.

5. Conclusions

[38] Velocities from a dense, continuous GPS network operating from 1999 to 2003 demonstrate that strain is accumulating across the Yucca Mountain area via $N20^\circ W$, right-lateral shear at a rate of 20 ± 2 nstrain/yr. The total velocity contrast across the network, the overall linearity of the velocity gradient, and the abrupt transition to underforming crust east of Yucca Mountain make it difficult to attribute the strain pattern solely to elastic bending of the crust adjacent to the Death Valley fault zone to the west. A significant fraction of the strain, equivalent to a structure with *contemporary* displacement rate in the 1 mm/yr range, may be present in the Yucca Mountain area. A simple model for strain accumulation on vertical strike-slip faults including 2.8 mm/yr on the Death Valley fault zone and 0.9 mm/yr on the Pahrump-Stateline fault, projected northward into the

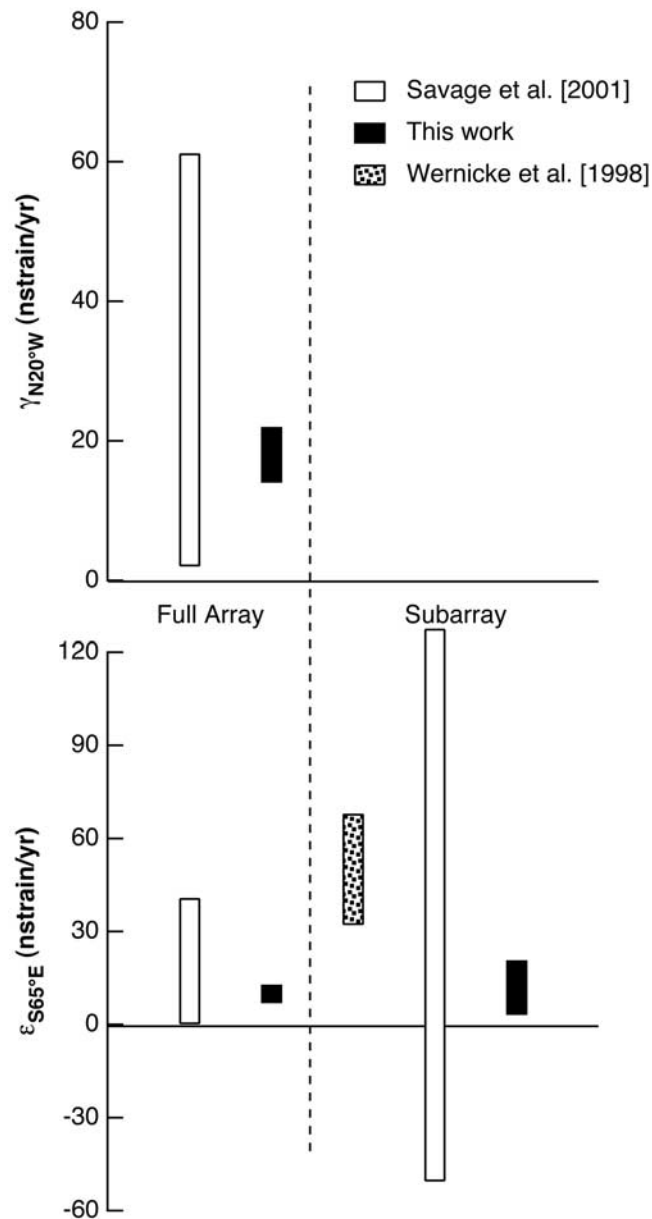


Figure 9. Comparisons of estimates of geodetic strain rate. Comparisons show range of values at 2 standard deviations, including estimates of (top) N20°W engineering shear strain and (bottom) S65°E elongation. Comparisons for the “full array” include the larger campaign network (aperture ~50 km) and the cluster of continuous sites reported on here, which cover approximately the same area. Results for the “subarray” include the smaller campaign network, a subset of sites from the larger campaign network, and a subset of sites from the continuous network.

Yucca Mountain area, provides a good fit to the geodetic data. However, other models, such as those invoking long-term seismic cycle effects, may also explain the data.

[39] In a period of less than four years, continuous monitoring has removed most of the uncertainty associated with previous campaign measurements by providing an estimate of the strain rate at 10 standard deviations that is significantly greater than geologic estimates, and by pro-

viding a useful upper bound on the spatial curvature of the velocity field that is inconsistent with intermediate- to far-field elastic bending. The new results are broadly consistent with the earlier campaign results, which have errors in NNW engineering shear strain rate that are a factor of 5 to 7 larger than the continuous results (Figure 9). The most notable difference with previous results, discussed earlier in the context of the baseline between sites WAHO and MILE, is the 50 ± 9 nstrain/yr elongation strain recorded on the temporally dense, local network from 1992 to 1997 [Wernicke et al., 1998]. Although consistent with highly uncertain results from a subset of sites from the larger campaign network, the difference with the overall result of 22 ± 9 is marginally significant at 2 standard deviations (28 ± 13 nstrain/yr), and the difference with the continuous network ($\sim 40 \pm 10$ nstrain/yr) is highly significant (Figure 9). The anomalously high rates may reflect, in part, accelerated postseismic strain following the 1992 Little Skull Mountain earthquake [e.g., Savage et al., 1999].

[40] Our results highlight the need for rigorous paleoseismic investigations of the Death Valley, Stateline-Pahrump and related fault zones, densification of continuous GPS sites across them, and improved modeling of the velocity field so as to take seismic cycle and other effects into account. Because of similarities in tectonic setting and contemporary deformation rate, earthquake scenarios along the lines of the 1932 Cedar Mountain event should be carefully considered in performance assessments of the proposed repository.

[41] **Acknowledgments.** This research was supported by DOE contract FC-08-98NV12081. Operation and analysis of the northern part of the BARGEN network was supported by NSF grants EAR-0135457 and EAR-0136102. Geodetic sites were constructed with technical assistance from the University NAVSTAR Consortium (UNAVCO) facility. Several of the figures were prepared using Generic Mapping Tools (GMT) version 3.4.2 [Wessel and Smith, 1998]. We are grateful to T. Herring for sharing calculations on postseismic effects of the Hector Mine earthquake in the Yucca Mountain area, and J. Price and G. Blewitt for discussions. We thank reviewers T. H. Dixon and J. C. Savage, and Associate Editor Y. Bock for constructive suggestions that substantially improved the quality of the manuscript.

References

- Anderson, L. W., R. E. Klinger, and D. S. Anderson (1997), Quaternary slip history of the Bare Mountain fault (Nevada) from the morphology and distribution of alluvial fan deposits, *Comment, Geology*, 25, 189.
- Beanland, S., and M. M. Clark (1994), The Owens Valley fault zone, eastern California, and surface rupture associated with the 1872 earthquake, *U.S. Geol. Surv. Bull.*, 1982, 1–29.
- Bell, J. W., C. M. dePolo, A. R. Ramelli, A. M. Sarna-Wojcicki, and C. E. Meyer (1999), Surface faulting and paleoseismic history of the 1932 Cedar Mountain earthquake area, west-central Nevada, and implications for modern tectonics of the Walker Lane, *Geol. Soc. Am. Bull.*, 111, 791–807.
- Bennett, R. A., J. L. Davis, P. Elósegui, B. P. Wernicke, J. K. Snow, M. J. Abolins, M. A. House, G. L. Stirewalt, and D. A. Ferrill (1997), Global Positioning System constraints on fault slip rates in the Death Valley region, California and Nevada, *Geophys. Res. Lett.*, 24, 3073–3076.
- Bennett, R. A., J. L. Davis, and B. P. Wernicke (1998), Continuous GPS measurements of contemporary deformation across the northern Basin and Range, *Geophys. Res. Lett.*, 25, 563–566.
- Bennett, R. A., J. L. Davis, J. E. Normandeau, and B. P. Wernicke (2002), Space geodetic measurements of plate boundary deformation in the western U.S. Cordillera, in *Plate Boundary Zones, Geodyn. Ser.*, vol. 30, edited by S. A. Stein and J. T. Freymuller, pp. 27–55, AGU, Washington, D. C.
- Bennett, R. A., B. P. Wernicke, N. A. Niemi, A. M. Friedrich, and J. L. Davis (2003), Contemporary strain rates in the northern Basin and Range province from GPS data, *Tectonics*, 22(2), 1008, doi:10.1029/2001TC001355.
- Bock, Y., et al. (1997), Southern California Permanent GPS Geodetic Array: Continuous measurements of regional crustal deformation between the 1992 Landers and 1994 Northridge earthquakes, *J. Geophys. Res.*, 102, 18,013–18,034.

- Bourne, S. J., P. C. England, and B. Parsons (1998), The motion of crustal blocks driven by flow of the lower lithosphere and implications for slip rates of continental strike-slip faults, *Nature*, 391(6668), 655–659.
- Davis, J. L., R. A. Bennett, and B. P. Wernicke (2003), Assessment of GPS velocity accuracy for the Basin and Range Geodetic Network (BARGEN), *Geophys. Res. Lett.*, 30(7), 1411, doi:10.1029/2003GL016961.
- Dixon, T. H., S. Robaudo, J. Lee, and M. C. Reheis (1995), Constraints on present-day Basin and Range deformation from space geodesy, *Tectonics*, 14(4), 755–772.
- Dixon, T. H., M. Miller, F. Farina, H. Wang, and D. Johnson (2000), Present-day motion of the Sierra Nevada block and some tectonic implications for the Basin and Range province, North American Cordillera, *Tectonics*, 19(1), 1–24.
- Dixon, T. H., E. Norabuena, and L. Hotaling (2003), Paleoseismology and Global Positioning System: Earthquake-cycle effects and geodetic versus geologic fault slip rates in the eastern California shear zone, *Geology*, 31, 55–58.
- Dokka, R. K., and C. J. Travis (1990), Role of the eastern California shear zone in accommodating Pacific-North American plate motion, *Geophys. Res. Lett.*, 17, 1323–1326.
- Friedrich, A. M., B. P. Wernicke, N. A. Niemi, R. A. Bennett, and J. L. Davis (2003), Comparison of geodetic and geologic data from the Wasatch region, Utah, and implications for the spectral character of Earth deformation at periods of 10 to 10 million years, *J. Geophys. Res.*, 108(B4), 2199, doi:10.1029/2001JB000682.
- Gan, W., J. L. Svarc, J. C. Savage, and W. H. Prescott (2000), Strain accumulation across the eastern California shear zone at latitude 36°30'N, *J. Geophys. Res.*, 105, 16,229–16,236.
- Hager, B. H., G. A. Lyzenga, A. Donnellan, and D. Dong (1999), Reconciling rapid strain accumulation with deep seismogenic fault planes in the Ventura basin, California, *J. Geophys. Res.*, 104, 25,207–25,220.
- Harmsen, S. C. (1994), The Little Skull Mountain, Nevada earthquake of 29 June 1992: Aftershock focal mechanisms and tectonic stress field implications, *Bull. Seismol. Soc. Am.*, 84, 1484–1505.
- Hearn, E. H., and E. D. Humphreys (1998), Kinematics of the southern Walker Lane belt and motion of the Sierra Nevada block, California, *J. Geophys. Res.*, 103, 27,033–27,050.
- Herring, T. A., J. L. Davis, and I. I. Shapiro (1990), Geodesy by radio interferometry: The application of Kalman filtering to the analysis of very long baseline interferometry data, *J. Geophys. Res.*, 95, 12,561–12,581.
- Hetland, E. A., and B. H. Hager (2003), Postseismic relaxation across the central Nevada seismic belt, *J. Geophys. Res.*, 108(B8), 2394, doi:10.1029/2002JB002257.
- Klinger, R. E., and L. A. Tietz (2000), Late Quaternary tectonic activity on the Death Valley and Furnace Creek faults, Death Valley, California, in *Geologic and Geophysical Characterization Studies of Yucca Mountain, Nevada, A Potential High-Level Radioactive-Waste Repository*, edited by J. W. Whitney and W. R. Keefer, *U.S. Geol. Surv. Digital Data Ser.*, 58, chap. H, 1–16.
- Langbein, J., F. Wyatt, H. Johnson, D. Hamann, and P. Zimmer (1995), Improved stability of a deeply anchored geodetic monument for deformation monitoring, *Geophys. Res. Lett.*, 22, 3533–3536.
- Lee, J., J. Spencer, and L. Owen (2001), Holocene slip rates along the Owens Valley fault, California: Implications for the recent evolution of the eastern California shear zone, *Geology*, 29, 819–822.
- Lohman, R. B., M. Simons, and B. Savage (2002), Location and mechanism of the Little Skull Mountain earthquake as constrained by satellite radar interferometry and seismic waveform modeling, *J. Geophys. Res.*, 107(B6), 2118, doi:10.1029/2001JB000627.
- McClusky, S. C., S. C. Bjornstad, B. H. Hager, R. W. King, B. J. Meade, M. M. Miller, and F. C. Monastero (2001), Present day kinematics of the eastern California shear zone from a geodetically constrained block model, *Geophys. Res. Lett.*, 28, 3369–3372.
- Menges, C. M., and J. W. Whitney (2002), Paleoseismic characterization of Quaternary faults at Yucca Mountain, Nevada, *Geol. Soc. Am. Abstr. Programs*, 34(6), 106–107.
- Meremonte, M., J. Gombert, and E. Cranswick (1995), Constraints on the 29 June Little Skull Mountain, Nevada earthquake sequence provided by robust hypocenter estimates, *Bull. Seismol. Soc. Am.*, 85, 1039–1049.
- Miller, M. M., D. J. Johnson, T. H. Dixon, and R. K. Dokka (2001), Refined kinematics of the eastern California shear zone from GPS observations, 1993–1998, *J. Geophys. Res.*, 106, 2245–2264.
- Niemi, N. A., B. P. Wernicke, A. M. Friedrich, M. Simons, R. A. Bennett, and J. L. Davis (2004), BARGEN continuous GPS data across the eastern Basin and Range province, and implications for tectonic system dynamics, *Geophys. J. Int.*, 159, 842–862, doi:10.1111/j.1365-246X.2004.02454.x.
- Reheis, M. C., and T. H. Dixon (1996), Kinematics of the eastern California shear zone, evidence for slip transfer from Owens and Saline Valley fault zones to Fish Lake Valley fault zone, *Geology*, 24, 339–342.
- Reheis, M. C., and T. L. Sawyer (1997), Late Cenozoic history and slip rates of the Fish Lake Valley, Emigrant Peak, and Deep Springs fault zones, Nevada and California, *Geol. Soc. Am. Bull.*, 109, 280–299.
- Savage, J. C. (2000), Viscoelastic-coupling model for the earthquake cycle driven from below, *J. Geophys. Res.*, 105, 25,525–25,532.
- Savage, J. C., M. Lisowski, W. K. Gross, N. E. King, and J. L. Svarc (1994), Strain accumulation near Yucca Mountain, Nevada, 1983–1993, *J. Geophys. Res.*, 99, 18,103–18,108.
- Savage, J. C., M. Lisowski, J. L. Svarc, and W. K. Gross (1995), Strain accumulation across the central Nevada seismic zone, 1973–1994, *J. Geophys. Res.*, 100, 20,257–20,270.
- Savage, J. C., J. L. Svarc, and W. H. Prescott (1999), Strain accumulation at Yucca Mountain, Nevada, 1983–1998, *J. Geophys. Res.*, 104, 17,627–17,632.
- Savage, J. C., J. L. Svarc, and W. H. Prescott (2001), Strain accumulation near Yucca Mountain, Nevada, 1993–1998, *J. Geophys. Res.*, 106, 16,483–16,488.
- Schweickert, R. A., and M. M. Lahren (1997), Strike-slip fault system in Amargosa Valley and Yucca Mountain, Nevada, *Tectonophysics*, 272(1), 25–41.
- Simons, M., Y. Fialko, and L. Rivera (2002), Coseismic deformation from the 1999 M_w 7.1 Hector Mine, California, earthquake as inferred from InSAR and GPS observations, *Bull. Seismol. Soc. Am.*, 92, 1390–1402.
- Smith, K. D., J. N. Brune, D. dePollo, M. K. Savage, R. Anooshehpour, and A. F. Sheehan (2001), The 1992 Little Skull Mountain earthquake sequence, southern Nevada Test Site, *Bull. Seismol. Soc. Am.*, 91, 1595–1606.
- Stewart, J. H. (1988), Tectonics of the Walker Lane belt, western Great Basin: Mesozoic and Cenozoic deformation in a zone of shear, in *Metamorphism and Crustal Deformation of the Western United States*, vol. 7, edited by W. G. Ernst, pp. 683–713, Prentice-Hall, Old Tappan, N. J.
- von Seggern, D. H., and J. L. Brune (2000), Seismicity in the southern Great Basin, 1869–1992, in *Geologic and Geophysical Characterization Studies of Yucca Mountain, Nevada, A Potential High-Level Radioactive-Waste Repository*, edited by J. W. Whitney and W. R. Keefer, *U.S. Geol. Surv. Digital Data Ser.*, 58, chap. J, 1–15.
- Wallace, R. E. (1987), Grouping and migration of surface faulting and variation in slip rates on faults in the Great Basin province, *Bull. Seismol. Soc. Am.*, 77, 868–877.
- Wdowinski, S., Y. Bock, J. Zhang, P. Fang, and J. Genrich (1997), Southern California permanent GPS geodetic array: Spatial filtering of daily positions for estimating coseismic and postseismic displacements induced by the 1992 Landers earthquake, *J. Geophys. Res.*, 102, 18,057–18,070.
- Wernicke, B., J. L. Davis, R. A. Bennett, P. Elósegui, M. Abolins, R. J. Brady, M. A. House, N. A. Niemi, and J. K. Snow (1998), Anomalous strain accumulation in the Yucca Mountain area, Nevada, *Science*, 279, 2096–2100.
- Wernicke, B., A. M. Friedrich, N. A. Niemi, R. A. Bennett, and J. L. Davis (2000), Dynamics of plate boundary fault systems from Basin and Range Geodetic Network (BARGEN) and geologic data, *GSA Today*, 10, 1–7.
- Wessel, P., and W. H. F. Smith (1998), New, improved version of generic mapping tools released, *Eos Trans. AGU*, 79, 579.
- Whitney, J. W., and D. L. Berger (2000), A 3.7-million-year offset rate on the Windy Wash fault at the south end of Yucca Mountain, Nevada, in *Geologic and Geophysical Characterization Studies of Yucca Mountain, Nevada, A Potential High-Level Radioactive-Waste Repository*, edited by J. W. Whitney and W. R. Keefer, *U.S. Geol. Surv. Digital Data Ser.*, 58, chap. F, 1–9.
- Whitney, J. W., and E. M. Taylor (Eds.) (1996), Quaternary paleoseismology and stratigraphy of the Yucca Mountain area, in *Seismotectonic Framework and Characterization of Faulting at Yucca Mountain, Nevada, Milestone Rep. 3GSHI00M*, chap. 4, U.S. Geol. Surv., Denver, Colo.
- Zhang, P., M. Ellis, D. B. Slemmons, and F. Mao (1990), Right-lateral displacements and the Holocene slip rate associated with prehistoric earthquakes along the southern Panamint Valley fault zone: Implications for southern Basin and Range tectonics and coastal California deformation, *J. Geophys. Res.*, 95, 4857–4872.

R. A. Bennett, Department of Geosciences, University of Arizona, Tucson, AZ 85721, USA.

J. L. Davis, Harvard-Smithsonian Center for Astrophysics, 60 Garden Street, MS 42, Cambridge, MA 02138, USA.

A. M. Friedrich, Institut für Geowissenschaften, Universität Potsdam, Karl-Liebknechtstr. 24/H25, D-14476 Golm, Germany.

N. A. Niemi and B. Wernicke, Division of Geological and Planetary Sciences, Mail Stop 100-23, California Institute of Technology, 1200 E. California Boulevard, Pasadena, CA 91125, USA. (brian@gps.caltech.edu)
J. E. Normandeau, University Navstar Consortium, 6350 Nautilus Drive, Boulder, CO 80301, USA.